Spatial focussing of wave energy for improved power capture by an oscillating water column

Robert Mayon and Dezhi Ning

Abstract—**Wave energy is a rapidly developing industry. However, its development and commercialisation is constrained by the low energy conversion efficiencies attained by the devices to capture the wave power. Minor advancements have been achieved by refining the geometry of the devices to capture the energy and the power-take-off systems. Nevertheless, the problem to deliver augmented energy densities to the wave energy conversion devices at source has not been resolved. If the hydrodynamic wave environment in the vicinity of the device can be augmented such that energy is focussed at that position, then a breakthrough may be achieved. This study aims to address this challenge. Here, the results of an investigation into the effects of wave energy focussing by various geometry reflector walls are presented. The incident waves and reflected waves interact with each other such that amplified positive and negative interference effectuates a hydrodynamic wave field with increased free surface displacements. Three disparate wall layouts, a parabolic concave wall, a straight oblique wall and a parabolic convex wall layout are investigated. In each case amplified free surface displacements are observed. A cylindrical oscillating water column is installed the wave field adjacent the three wall geometries and the hydrodynamic conversion efficiencies are recorded over a range of wave conditions. The results are compared with an equivalent oscillating water column in open-seas conditions. Significantly augmented energy conversion efficiencies are demonstrated. Furthermore, the manipulated hydrodynamic wave field observed may be advantageous for the deployment of an array system of wave energy convertors.**

Keywords—**Wave energy focussing, wave reflection, oscillating water column, constructive wave interference.**

I. Introduction

IN recent years there has been a marked acceleration in the development of renewable energy technologies. This has been primarily driven by the rising prices in fossil fuels and to an extent, in the renewed focus on environmental considerations. It is recognised that the worlds' oceans are a vast repository of clean and renewable energy and research into marine energy systems has been expedited lately.

Whilst tidal energy devices are at a reasonably advanced stage, the wave energy sector is still in the developmental phase. The potential of wave energy is immense- it is estimated at approximately 29,500 TWh/yr [1]. Of this resource, approximately up to 2.2 TW of wave power is incident upon ocean-facing coastlines [2]. Moreover, wave energy has the advantageous characteristics of being relatively spatially and temporally stable.

Research into all aspects of wave energy from the primary conversion stage to the power-take-off (PTO) systems is continuing apace and there have been a large number of prototype wave energy converter (WEC) devices developed and deployed [3]. Of these devices, the oscillating water column (OWC) is considered one of the most promising categories of WEC due to its simplicity of operation. Indeed there are a small number of grid-connected commercial installations in operation- with the Mutriku, Yongsoo, and REWEC3 power plants being well known examples. These are all instances of the OWC WEC.

However, whilst a few full-scale installations have been constructed, an extensive commercialisation of wave energy technology has not been realised and most projects are at a moderate technology readiness level (TRL). The reasons for this are manifold, but the predominant challenge associated with OWC WECs is attributed to the low energy conversion at the primary harvesting stage. The majority of OWCs that have been developed from laboratory scale to full scale, exhibit low first stage energy conversion, with an average Capture Width Ratio (CWR) of 29% [4]. Further energy losses occur at the secondary

Sponsor and financial support acknowledgement: This work was supported by the National Natural Science Foundation of China (Grant Nos. 52250410362, 52271260 and U22A20242) and by the Innovation Fund for Young Scholars of the State Key Laboratory of Coastal and Offshore Engineering, Dalian University of Technology (Grant No. LY206).

R. M. Author is with the State Key Laboratory of Coastal and Offshore Engineering, Dalian University of Technology, Dalian, 116024, China, and at Dalian State Key Laboratory of Offshore Renewable Energy, Dalian University of Technology, Dalian, 116024, China (e-mail: rmayon@dlut.edu.cn).

D. N. Author is with the State Key Laboratory of Coastal and Offshore Engineering, Dalian University of Technology, Dalian, 116024, China, and at Dalian State Key Laboratory of Offshore Renewable Energy, Dalian University of Technology, Dalian, 116024, China (e-mail: dzning@dlut.edu.cn).

Digital Object Identifier: https://doi.org/10.36688/ewtec-2023-266

energy conversion stage, i.e. at the PTO system, resulting in wave-to-wire conversion efficiencies lower the 10% for OWCs.

In other renewable energy capturing systems the source energy is usually concentrated at the energy harvester; for example Orbital Marine Power's tidal turbine exploits the natural terrain topology around the Orkney Islands where there is a high tidal potential for maximum energy capture. Likewise wind turbine farms are occasionally constructed in regions where natural mountainous slopes deliver increased wind energy densities, and solar farms employ vast fields of reflectors to concentrate the solar power to a central collector.

This energy focussing concept has not been adopted in an analogous manner to the wave energy sector. This research aims to address the challenges associated with the low energy conversion efficiencies observed at OWC WECs, especially at the primary stage. By coupling an OWC with a reflecting wall structure, enhanced wave energy conversion can be achieved. The system operates by reflecting the incident wave in such a manner that the reflected and incident waves interfere with each other to effectuate amplified free surface displacements. Then, an OWC WEC can be installed at these focussed wave positions.

Whist there have been many studies on the efficacy of breakwaters for wave attenuation or wave reflection, fewer investigations have been conducted with the explicit aim of determining wave focussing effects by a reflecting wall for the purpose of wave energy harvesting. Those that have been conducted usually examine the effects of incident wave propagation and reflection normal to the breakwater. A few prior studies in which wave interactions with more complex reflecting wall are investigated are presented here. Zhang and Ning [5] performed a numerical investigation using the boundary element method on a novel breakwater geometry consisting of a straight wall with multiple parabolic openings. They found that the wave height at the focus point of the parabolic opening can reach up to four times the incident wave height. They also investigated the influence of the distance between neighbouring parabolic openings and found that as the distance increases the maximum wave height at the parabolic opening focus point decreases. The authors incorporated an oscillating buoy type WEC into the numerical domain and observed that the heave response can be amplified by a factor of three by the parabolic reflecting wall. Ren et al., [6] performed a parametric analysis on a parabolic arc pontoon breakwater for the purpose of investigating the wave attenuation and focussing at the leeward and wave-ward sided respectively. They observed a critical frequency at which optimal attenuation and focussing occurred. In their parametric analysis, they found that increasing the draft strongly influenced the critical frequency with little effect on the wave attenuation performance. Subsequently they found that increasing the chord length provided a beneficial effect to the wave energy focussing performance. They observed a wave amplification rate of approximately 3, and a wave attenuation rate of approximately 68% in front of, and behind the breakwater respectively. Zhou et al., [7] investigated the use of a system of parallel twin parabolic floating breakwaters for the purpose of wave attenuation on the lee side, and wave focussing at the weather side of the breakwater. They employed the potential flow theory to investigate the influence of gap spacing between the breakwaters and the breakwater connection method on the hydrodynamic flow field. The authors found that a rigid connection between the breakwater walls performed better than unconnected walls, yielding better wave attenuation at the leeward side and better wave focussing on the weather side of the structure. They also observed a critical gap width for wave attenuation. Later, Zhou et al., [8] investigated the performance of a pair of side by side parabolic breakwaters, again they investigated the gap distance between the breakwaters and the connection method. They found that for a non-zero gap distance, a rigid connection yielded beneficial wave amplification on the weather side of the breakwater. These few studies listed demonstrate the capacity for achieving beneficial effects by installing an intelligently designed reflecting wall in the incident wave field. These previous studies were all conducted using the potential flow theory.

This research advances the earlier investigations by employing a fully nonlinear CFD model to investigate wave field amplification, and accordingly, energy coalescence by three different reflecting wall layouts. Wave reflection at the concave side of parabolic wall, at the convex side of a parabolic wall and finally at a wall positioned obliquely to the propagating incident wave are examined over a range of incident wave conditions. Finally an OWC WEC is installed in the domain and the hydrodynamic efficiencies are presented. All numerical simulations are conducted using the open-source CFD software OpenFOAM.

II. NUMERICAL DOMAIN

A. *Geometry*

This study investigated the effects of wave reflection for energy coalescence at three different wall layouts; a concave parabolic wall, a convex parabolic wall and a straight oblique wall as shown in Figure 1. The numerical domain geometry was selected to duplicate an experimental study which was performed on the concave parabola reflecting wall layout at the State Key Laboratory of Coastal and Offshore Engineering, Dalian University of Technology. The maximum domain length was 29.7 m measured from the wave generation boundary to the

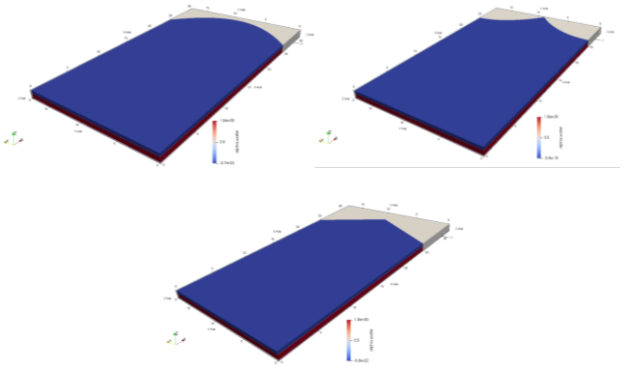

Fig. 1. Domain geometries with varying reflecting wall layouts.

parabola apex. This distance is also set as the maximum domain length with the convex parabola and oblique wall setup. The domain width is set as 18.00 m and the water depth in the numerical tank is set to 0.6 m. The concave parabola reflecting wall is designed with a sagitta distance of 4.8 m and a focal distance of 4.222 m. The convex parabola reflecting wall setup is achieved by mirroring the concave parabola about the Y-axis. In order to achieve wave focussing effects in the convex wall setup, two halves of the convex parabola are joined at the position where the parabola intersects the sagitta distance (see Fig. 1). During the course of the study it was found that an oblique wall positioned at an angle of 45° to the incident wave did not effectuate optimal wave focussing in the along-wave direction (i.e. in the direction perpendicular to wave propagation direction). This was due to viscous fluid effects at the interaction of the incident and reflected waves. It was found that a wall aligned at approximately 62° to the direction of wave propagation reflected the waves with a propagation direction perpendicular to the incident wave direction. This resulted in a checkerboard type wave field focussing configuration (See Fig. 2).

III. MATHEMATICAL FORMULATION

The parabolic opening was defined in the *x,y* plane using the coordinate system *O-xyz* according to:

$$y^2 = -2a(x - x_0), \tag{1}$$

where a is coefficient which determines the curvature of the parabolic opening, The vertex of the parabolic opening is at $\{x_0, 9\}$, where $x_0 = 29.7$. In this study the parabolic opening is designed with an aspect ratio of 3.75.

The initial stage of the research investigating wave focussing in the absence of the OWC chamber was conducted using the incompressible dual phase solver interFoam. The fluid flow governing equations in partial differential form are:

$$\nabla \cdot \boldsymbol{U} = 0, \tag{2}$$

where ∇ is the gradient operator and $\boldsymbol{U}$is the flow velocity vector.

$$\frac{\partial \rho \boldsymbol{U}}{\partial t} + \nabla \cdot (\rho \boldsymbol{U}\boldsymbol{U}) = \nabla \cdot \boldsymbol{\tau} + \rho \boldsymbol{b}, \tag{3}$$

where ρ is the fluid density, $\boldsymbol{\tau}$ is a viscous stress tensor and $\boldsymbol{b}$ denotes body forces acting on a control volume.

Later, subsequent to the installation of the OWC chamber the compressible dual phase solver compressibleInterFoam was utilised. A previous study on wave energy capturing by a cylindrical OWC chamber at a concave parabolic wall determined that the air-phase compressibility effects in the pneumatic chamber were significant even at this laboratory scale. This is due to the large mass of water concentrically converging upon the chamber which effectuated large free surface displacements inside the chamber (relative to the incident wav height) which accelerated rapidly. Then, in this second part of research in which compressibility effects were found to be significant inside the OWC chamber due to the rapid and relatively large scale volumetric change in air phase, the energy conservation equation was included as an additional constraint,

$$\frac{\partial \rho h_e}{\partial t} + \nabla \cdot (\rho h_e \boldsymbol{U} + \boldsymbol{q}) = \nabla \cdot (\boldsymbol{\tau}\boldsymbol{U}) + \boldsymbol{U} \cdot \rho \boldsymbol{b}, \tag{4}$$

where h_e is the system enthalpy and $\boldsymbol{q}$ is the heat flux vector.

The dynamic free surface was tracked using the Volume Of Fluid (VOF) method. Using this technique, a transport equation is defined,

$$\frac{\partial \alpha}{\partial t} + \nabla \cdot (\mathbf{U}\alpha) = 0, \tag{5}$$

where α is the cell volume fraction.

In the second part of the study investigating the performance of the OWC chamber installed in each of the three respective domain geometries, the hydrodynamic efficiency was used as a performance metric for determining the efficacy of the OWC WEC to capture energy at each of the reflecting wall geometries. The hydrodynamic efficiency is defined as,

$$\xi = \frac{P_o}{P_w w}, \tag{6}$$

where P_o is OWC hydrodynamic power output, P_w is the incident wave power and w is the characteristic width of the OWC. In this study a cylindrical OWC is employed for energy harvesting and therefore the internal chamber diameter is taken as the characteristic width. Although the incoming waves are incident upon the various wall geometries and are reflected back into the domain, the as the wave propagates down the domain it is only incident upon the width of the OWC chamber, therefore selecting the chamber diameter and not the reflecting wall width as the characteristic width is a reasonable assumption. The OWC hydrodynamic power can be calculated from,

$$P_o = \frac{1}{T}\int_t^{t+T} Q(t)p(t)dt, \quad (7)$$

where T is the incident wave period, Q is the volumetric air flux through the OWC chamber orifice and p is the chamber aerodynamic pressure.

According to linear wave theory, the incident wave power is given as,

$$P_w = \frac{1}{2}\rho g A_i^2 C_g, \quad (8)$$

where g is gravity acceleration, A_i is the incident wave amplitude and C_g is the incident wave packet group velocity calculated from,

$$C_g = \frac{c}{2}\left(1 + \frac{2kh}{\sinh 2kh}\right), \quad (9)$$

where k is the wave number, h is the static water depth and c is the incident wave velocity calculated from,

$$c = \frac{\omega}{k}. \quad (10)$$

ω is the angular wave frequency given by,

$$\omega = \sqrt{gk \tanh kh} \quad (11)$$

Using equations 1-11 presented above the wave propagation can be simulated and the hydrodynamic efficiency of the cylindrical OWC can be computed.

IV. RESULTS

A. *Wave energy focussing*

The results for the wave energy focussing study are first presented. Figure 2 depicts an image of the focussed wave pattern for each of the various wall layouts for wave conditions H = 0.05 m, T = 1.4 s. This section discusses the wave energy focussing with respect to the maximum free surface displacements observed and the limits of the region in which wave amplification is recorded. Here we consider the energy focussing in the domain region X ≥ 20m. The parabolic wall configuration demonstrates the optimal monopole, wave focussing with a maximum free surface displacement at the focal position of 0.74 m. The incident wave amplitude is 0.025 (yielding a free surface elevation in the absence of focussing of 0.625 m) and thus a free surface displacement amplification of 5.6 is achieved through the addition of the parabolic wall. The maximum amplifications are more moderate for the convex parabolic wall and for the oblique wall configurations yielding amplification factors of 3.2 and 3.6 for the convex and oblique walls respectively. Interesting observations can be determined from a qualitative analysis of the wave focussing patterns demonstrated on Figure 2. The concave parabolic wall clearly focusses the greater part of the reflected wave energy towards the parabolic focus position at the expense of amplified free surface displacement in the remaining regions of the domain. This denotes the concave parabolic wall coalesces the energy to a single point and is a particularly suitable reflecting structure for wave energy focussing in conjunction with the deployment of a single WEC. Furthermore, there is relatively little free surface amplification in the region X<12 m.

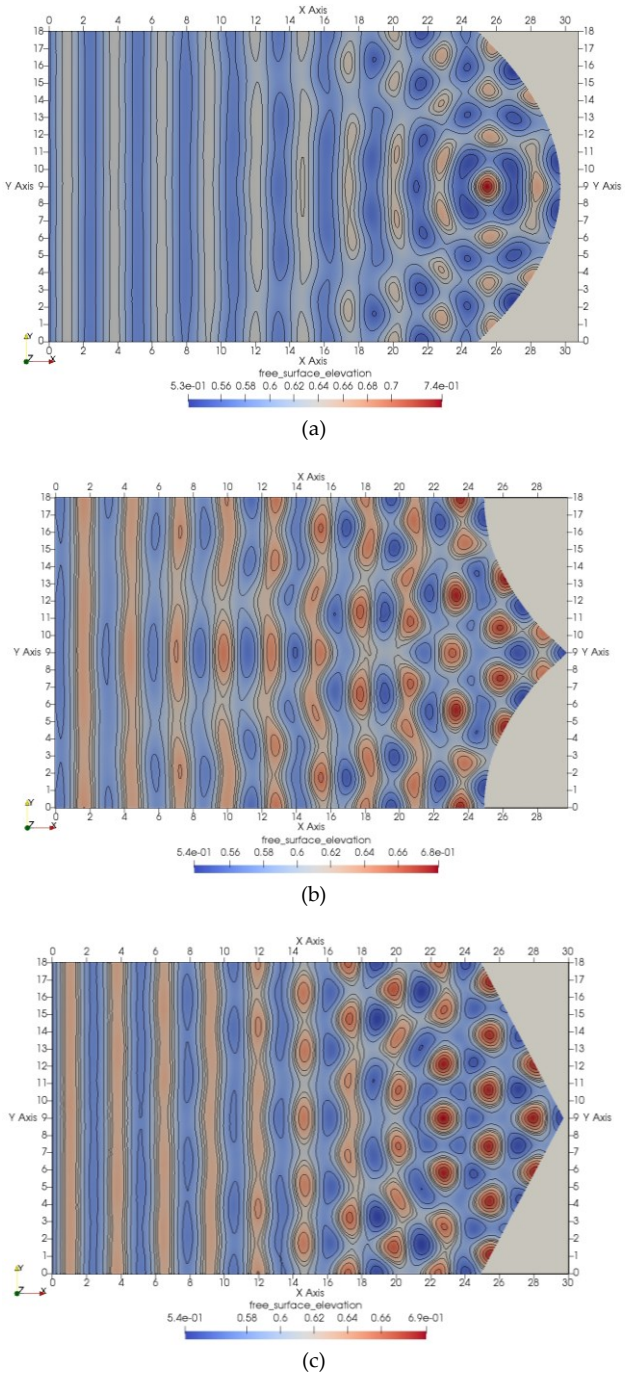

Fig. 2. Free surface contours demonstrating wave focussing configuration (a) wave focussing at a concave parabolic wall, (b) wave focussing at a convex parabolic wall, (d) wave focussing at an oblique wall.

With regards to the convex parabolic wall layout, the maximum free surface displacement is less than that of the parabolic concave wall configuration, however the wave energy focussing distribution is more uniform. Instead of

the preponderance of the incident and reflected wave energy being focussed to a single point, a number of focussing positions now manifests. None of these energy focussing regions reach the level of displacement observed with the concave parabolic wall, however because there are more focussing positions, the energy is distributed more uniformly throughout the domain and this configuration may be suitable for the deployment of a WEC array. Furthermore, it can be seen that the waves are reflected further back down the domain in the negative X direction resulting in wave interference and associated free surface amplification in the region of X>6.

Finally, the oblique wall geometry exhibits performance somewhat intermediate to the two previous cases. The maximum free surface displacement is greater than that of the convex parabolic wall layout but less than the concave parabolic wall. Conversely, the free surface amplification region is greater than the concave parabolic wall but less than that of the convex parabolic wall, with amplified free surface displacements observed in the region X>8 m.

Figure 3 demonstrates the cause of the various wave amplification topologies for each of the wall geometries. The incident wave propagation direction is highlighted with red arrows. The crests of the incident waves are highlighted in red bold dashed lines. The reflected wave propagation direction is demonstrated by the yellow arrows and the reflected wave crests are depicted by the yellow bold dashed lines. The reflected waves in the concave parabolic geometry propagate with negligible velocity in the negative x direction (in the region between the wave generation boundary and the parabola focus point), whereas in the convex parabolic case the waves are reflected predominantly in the negative x direction. The waves are reflected primarily in the y direction in the oblique wall simulation.

Next we consider the temporal and spatial distribution of the incident and reflected wave energy in a qualitative manner. In the case of a plane unidirectional propagating wave, it is a trivial matter to calculate the energy of the wave according to Equation 8 above. However, because of the complex hydrodynamic wave field generated by the incident and reflected wave interference, it is difficult to determine the wave energy quantification and distribution in the present model domains. A further complexity is introduced as the irregular free surface experiences a dynamic topology with time-varying elevations at different spatial locations due to the propagation of the incident and reflected waves. Here, it is postulated that the displaced volume of water and the topology of the free surface can be used as a proxy for the energy distribution in the domain.

By truncating the free surface at the SWL, and at regular intervals above the SWL (in the z-direction) the energy distribution can be qualitatively determined. The process is outlined below using the incident wave with period T=1.8 and the three wall geometries as the example.

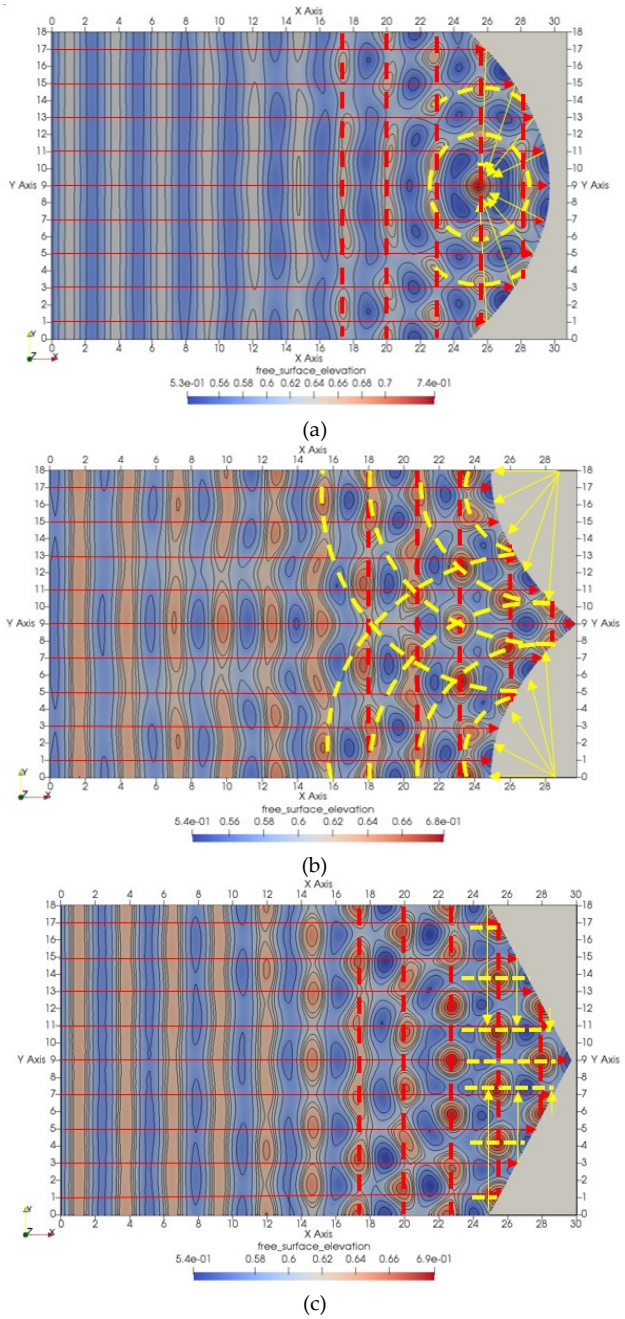

Fig. 3. Wave energy focussing mechanisms at each of the reflecting wall geometries

The water free surface is truncated at the SWL (0.6 m), and incrementally above the SWL. At each threshold truncation level, ζ, the total free surface areas above each threshold is extracted from the simulation data. These time varying areas are presented in Figure 4 for each of the three domain geometries with the incident wave period T = 1.8 seconds.

From Figure 4 it can be seen that in the case of the concave wall, the free surface area above the SWL oscillates with a periodicity matching that of the incident wave period (with a slight phase shift). This single-harmonic oscillation is due to the fact that the substantial part of the energy is focussed to a single position, i.e. the focal point of the concave opening. The maximum and minimum area values are anti-phasic with respect to the

maximum and minimum surface elevations at the focal position. This is demonstrated on Figure 5.

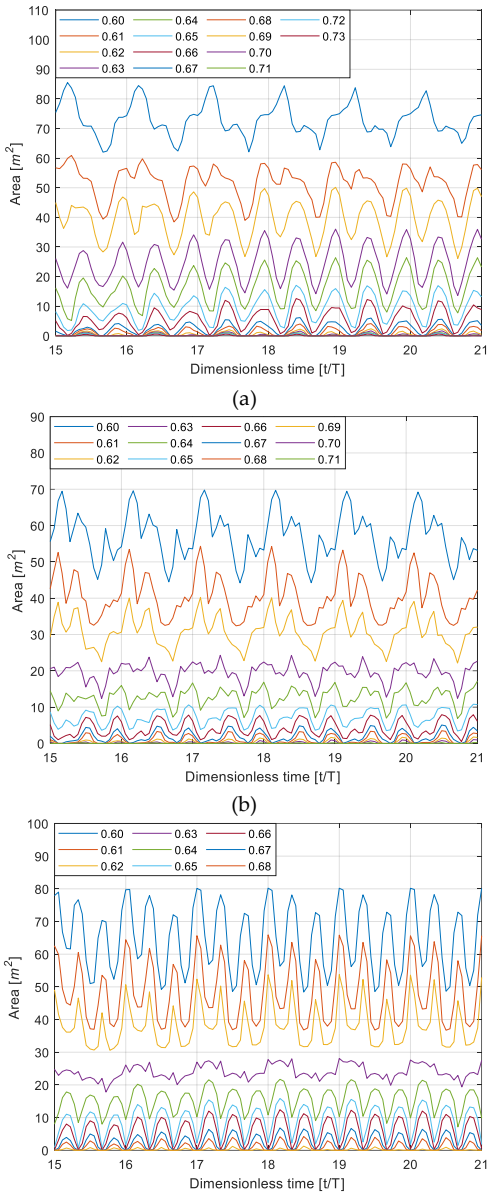

Fig. 4. Time varying total free surface areas above threshold truncations for incident wave period T = 1.8s. (a) concave wall simulation, (b) convex wall simulation, (c) oblique wall simulation

As the threshold truncation level is increased above the SWL, the free surface areas above the threshold reduces, but the time varying free surface area now oscillates with a bi-harmonic behaviour as demonstrated when the threshold is set to 0.64 m (Fig. 4(a)). The free surface area reaches a maximum at the corresponding times when surface displacement is at its maxima and minima. This demonstrates that the areal oscillation at the higher threshold values transitions to being in-phase with respect to the maximum and minimum elevation displacements of the free surface. This is caused by the fact that the free surface area exceeding this elevated threshold is more uniformly distributed in the domain. Thus, instead of the majority of the energy coalescing around the focal point as occurs lower threshold elevations, at these higher threshold elevations the energy is distributed within the parabolic opening. Finally, at the upper threshold truncation elevations (z > 0.70), the oscillatory free surface area reverts to a monoharmonic oscillation in phase with the maximum free surface elevation displacements, this occurs because only one region of the free surface exceeds these upper threshold elevations, (i.e. the region around the focal point) (see Figure 6).

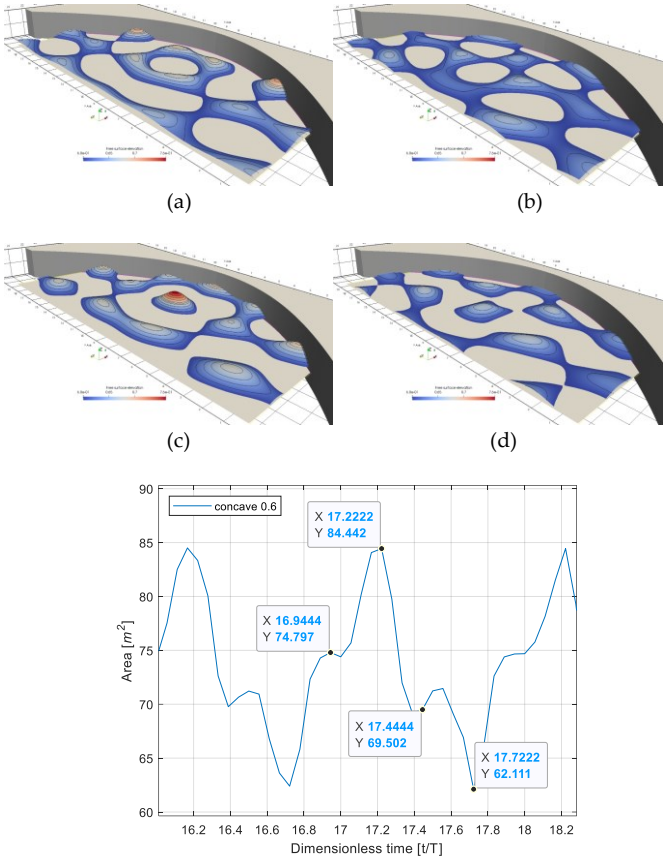

Fig. 5. Concave simulation free surface area above SWL (indicated by the grey plane). (a) non-dimensional simulation time 16.94, (b) non-dimensional simulation time 17.22, (c) non-dimensional simulation time 17.44, (d) non-dimensional simulation time 17.72, (e) area fluctuation above SWL (at 0.6 m).

A similar analysis procedure can be applied to the convex and oblique wall simulations. As the convex wall time varying free surface area variation is similar to that of the concave wall simulation and it will not be analysed in detail. However it is notable that the oblique wall simulation effectuates disparate behaviour in the time varying free surface areal distribution. As shown on Figure 4(c), the time varying area oscillates with a multi harmonic periodicity above all threshold elevations. Whilst the maximum free surface displacement does not reach the displacement values observed with the concave parabolic wall, the free surface oscillates more energetically at the lower elevations. This is evidenced by the greater number of, and more uniformly distributed focussing positions in in the oblique wall simulation setup.

In order to qualitatively compare the time varying areas (as presented in Fig. 4) for each wave period and each reflecting wall geometry, the time averaged areas over a single wave period is calculated, and the results are then plotted as a three dimensional surface plot as shown in

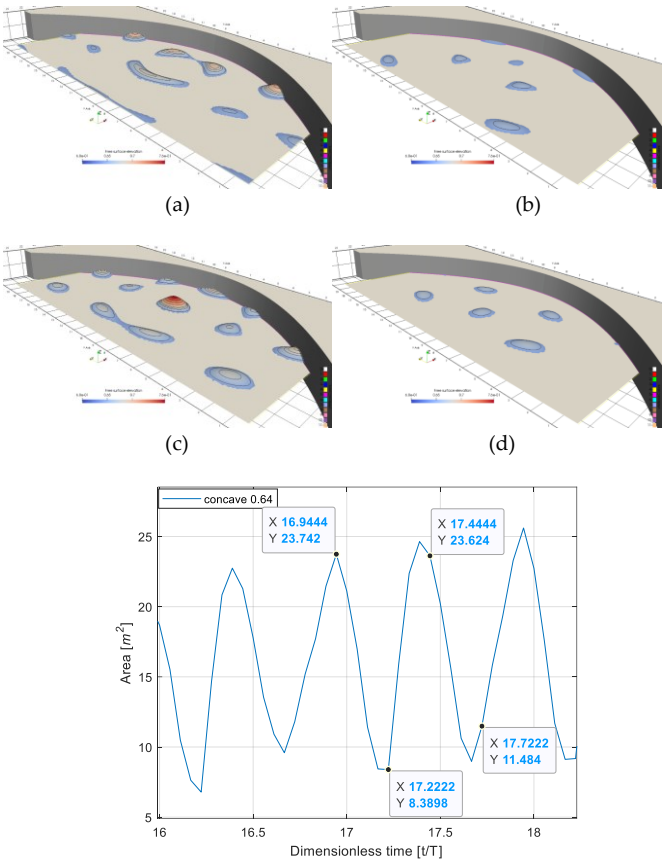

Fig. 6. Concave simulation free surface area above 0.64 m (indicated by the grey plane). (a) non-dimensional simulation time 16.94, (b) non-dimensional simulation time 17.22, (c) non-dimensional simulation time 17.44, (d) non-dimensional simulation time 17.72, (e) area fluctuation above SWL.

Figure 7. Here we only present the results for the areal distribution above the threshold for the range $0.6 \leq \zeta \leq 0.66$, as the areas above the upper limit of this threshold are relatively small. It is notable that the areal distributions follow a similar trend for each of the investigated geometries with the concave parabolic wall geometry producing higher areal values above each threshold, followed by the oblique wall simulation and finally the convex parabolic wall simulation. It is also conspicuous that incident wave period T = 1.6 seconds yields higher areal values at each of the geometries (it is shown later that the maximum power output from an OWC in the concave and convex parabola geometries occurs at incident wave period, T = 1.8 seconds). The oblique wall geometry simulation also exhibits contrasting behaviour to the other simulation setups at the higher incident wave periods in which the area does not decrease at the upper threshold heights.

The same procedure as outlined for analysing the areal distribution is applied to the volumetric distribution, and the time varying volume above each of the threshold elevations is be extracted from the simulations. For brevity, only the volumetric comparison for each of the simulation geometries will be presented as shown in Figure 8. Similarly with the concave areal distribution case, the volumetric distribution of water displaced at wave period T = 1.6 seconds is equivalent to that displaced at T = 1.8 seconds. On inspection of the OWC power curve for the case of the convex parabolic wall it can be seen that

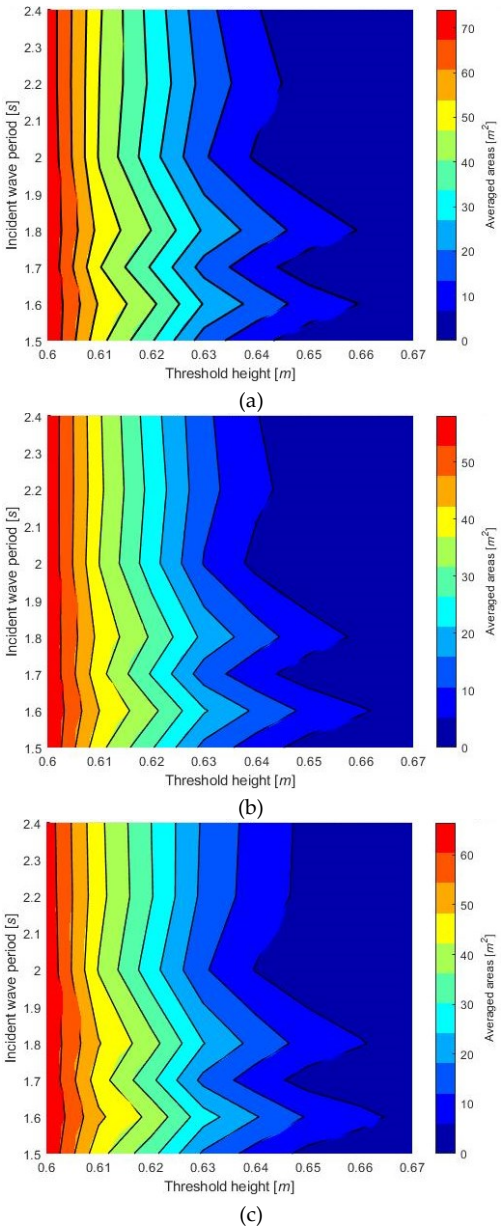

Fig. 7.Area comparison above threshold levels for each simulation setup. (a) concave wall simulation, (b) convex wall simulation, (c) oblique wall simulation

there are two local maximums occurring at T = 1.6 seconds and at T = 1.8 seconds. The greater volumetric displacement of water at theses two wave conditions contribute to these power maxima. Furthermore, since the simulations show that the greatest free displacement occurs at the focal point in the concave wall simulation it is clear that the energy is then coalescing at this point.

In the case of the oblique wall simulations, the volume of water displaced at T = 1.6 seconds is consistently greater than the volume displaced at T = 1.8 seconds (supporting the fact that the greatest hydrodynamic power capture by the OWC occurs at this wave condition). Furthermore, the areal distribution at the higher threshold elevations is greater in the wave period case of T = 1.8 seconds. Then it can be ascertained that a larger volume of water

distributed over a larger area results denotes that the wave energy is more uniformly distributed in the domain. Further and more in-depth analysis can be performed on the energy field distribution at the three wall geometries, however only a brief synopsis is presented herewith.

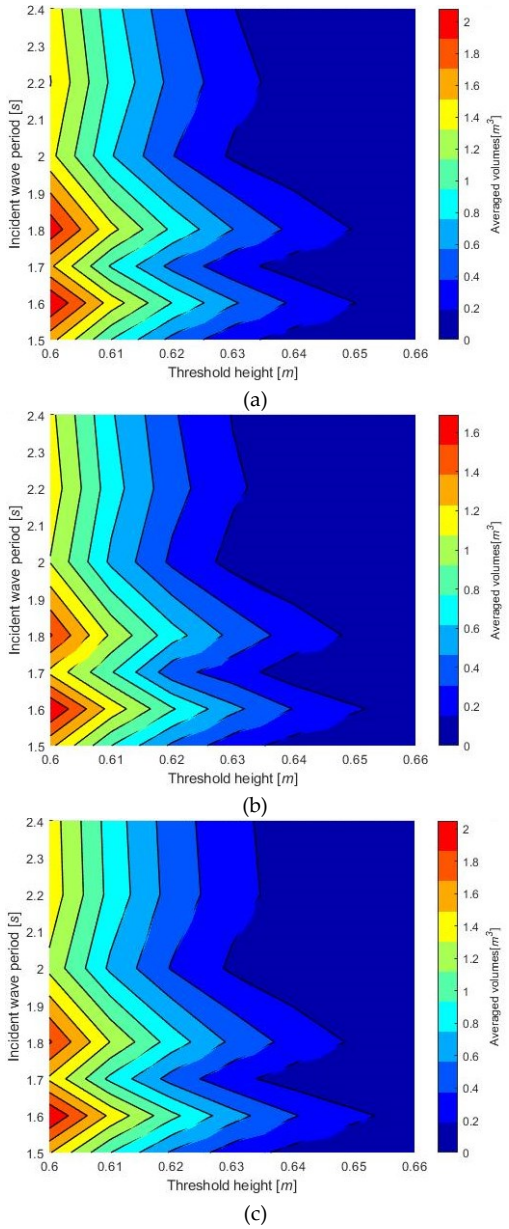

Fig. 8. Area comparison above threshold levels for each simulation setup. (a) concave wall simulation, (b) convex wall simulation, (c) oblique wall simulation

B. *Wave energy capture by OWC at different geometry walls*

Subsequent to the analysis of the capacity of the various geometry reflecting walls to focus the wave energy, a cylindrical OWC WEC was installed in each of the three numerical domains. The spatial positioning of the OWC was determined with reference to the concave parabolic wall geometry. The OWC chamber was installed with its axisymmetric centreline coincident with the parabolic wall focal point. The location of OWC in both the convex parabolic and oblique wall model geometries was identical to that of the concave geometry with regards to the distance from the wave inlet boundary and the distance to the wall apices. According to the earlier analysis of wave focussing, it is to be expected that the OWC chamber installed adjacent to the concave parabolic wall will exhibit the maximal power capture as the preponderance of the reflected wave energy in the numerical domain is directed towards the focal position. It was unbeknownst which of the oblique wall or the convex parabolic wall simulations would demonstrate the greater power capture *a priori* to the analysis as both geometries effectuate locally distributed wave energy focussing in the domain vicinity adjacent the walls. The OWC hydrodynamic efficiency is calculated according the chamber air-phase volumetric change and the chamber aerodynamic pressure as demonstrated by Equation 7. The time varying volume can be correlated to the chamber free surface displacement.

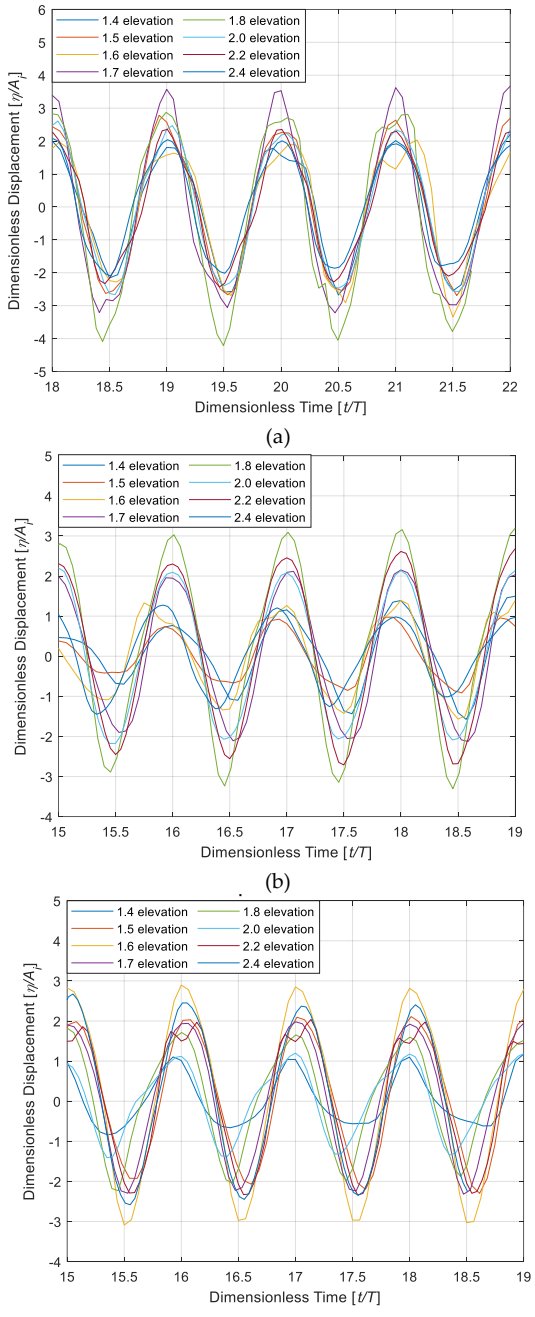

Fig. 9. Time varying free surface displacements within the OWC chamber. (a) concave wall simulations, (b) convex wall simulations, (c) oblique wall simulations.

Figures 9 and 10 present the results of the time varying free surface displacement and the pressure variation in the chamber for each of the three geometries respectively.

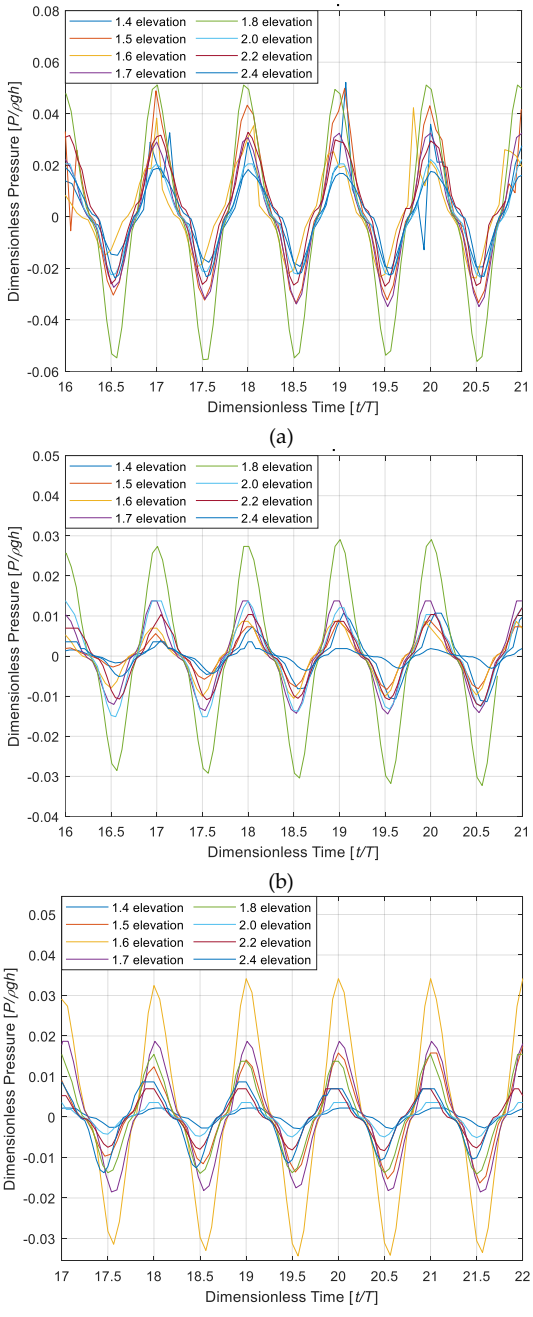

Fig. 10. Time varying aerodynamic pressures within the OWC chamber. (a) concave wall simulations, (b) convex wall simulations, (c) oblique wall simulations.

In Figure 9 the abscissa axis has been non-dimensionalised by the wave period and the ordinate axis has been non-dimensionalised by the wave amplitude. The concave parabolic wall geometry instigates a greater free surface displacement with the other two simulation geometries attaining similar chamber free surface displacements. However, it is notable that there this a phase shift in the case of the oblique wall geometry setup with the maximal free surface displacements occurring at incident wave period T = 1.6 seconds whereas in the other two geometries the maximum free surface displacement occurs with wave period T = 1.8 seconds. This phase shift may be explained by the varying wave focussing mode which is observed with the oblique wall setup.

Figure 10 presents the associated chamber pressures for each of the numerical simulation cases shown in Figure 9. Again, the abscissa axis is non-dimensionalised by the incident wave period and the ordinate axis has been non-dimensionalised by the hydrostatic pressure, P_{hyd} at the base of the wave tank (i.e., $P_{hyd} = \rho g h$, where h is the SWL).In the case of the concave wall simulations, the greatest pressure range occurs at the T=1.8 second simulation. However, the chamber pressures recorded during the simulation cases with the other incident wave periods do not vary greatly from each other, nor from the maximum pressure range. In contrast, the pressures recorded during the convex wall simulation exhibit more variance. The aerodynamic pressure measured during the T = 1.8 second simulation is significantly greater than the pressures observed at the other incident wave period simulations. In the case of the oblique wall simulations, the Maximum pressure is recorded during the T= 1.6 second incident wave period and again this dynamic pressure is notably larger than the pressures measured during the other incident wave period simulation cases. These pressure result behaviours at each of the wall geometries and incident wave periods are in good concordance with the free surface displacement behaviours presented in Figure 9.

Following on from the computation of the chamber volumetric air fluxes and the chamber pressures, the hydrodynamic power at each simulation geometrical configuration and incident wave period can be calculated. Figure 11 presents the hydrodynamic power for each numerical simulation case. Also included in Figure 11 is the incident wave power. It should be noted that an experimental investigation on the concave parabolic wall geometry was performed contemporaneously with the numerical simulation investigation. However this study presents the results from the numerical study only. Nevertheless, Figure 11 also includes the hydrodynamic power results obtained from the experimental investigation for validation of the numerical results obtained. In Figure 11 it can be seen that the concave wall geometry setup yields the greatest hydrodynamic power. The maximum power is generated at incident wave period T = 1.8 seconds, in agreement with the chamber pressure and free surface displacement results.

Furthermore, the concave wall setup results in greater hydrodynamic power output than that of the incident wave. This is a notable observation. The concave parabolic wall concentrates the incident and reflected wave energy to the focal point effectuating a localised point-power density greater than the linearly distributed power along the propagating incident wave front. The OWC hydrodynamic power output surpasses the incident wave power in the range of T<1.9 seconds. This large effective bandwidth with high power outputs also demonstrates the efficacy of the proposed system. wave for equivalent wave

conditions. The numerical simulation results obtained during the concave parabolic wall simulation shows good agreement with the experimental investigation. The results obtained from the convex parabolic wall and the oblique wall simulations present more moderate hydrodynamic power outputs. Neither set of results attain the level of the incident wave power. The maximum power achieved at convex parabolic wall setup occurs at the same resonant wave period as the concave wall setup (T = 1.8 seconds); however, in the case of the oblique wall geometry, the resonant period is downshifted to T = 1.6 seconds. Furthermore, the effective bandwidth is narrowed in the convex parabolic wall geometry simulations compared with the concave wall setup, and to a greater extent in the case of the oblique wall geometry.

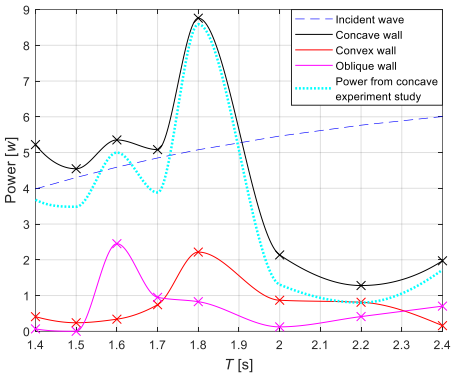

Fig. 11. Hydrodynamic power outputs for each geometrical setup

The reason for the reduced hydrodynamic power output in the case of the oblique wall can be ascertained from Figure 2. This figure clearly shows that the wave energy is focussed to many localised positions with the oblique wall, in contrast with the focussing mechanism at the concave parabolic wall in which the energy coalesces to a single point. These observations support the hypothesis that reflecting walls can be employed to manipulate the wave field to concentrate the wave energy at a single point location for the installation of a single WEC or to multiple point locations for the installation of a WEC array.

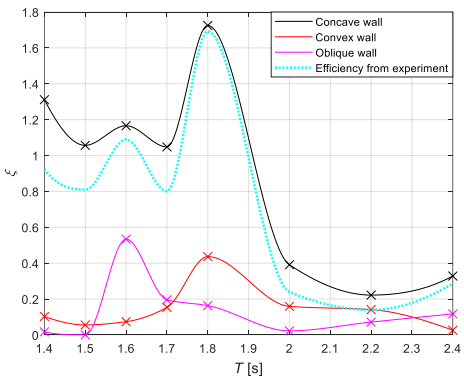

Fig.12. Hydrodynamic power outputs for each geometrical setup

Finally, Figure 12 presents the hydrodynamic efficiency obtained from the numerical simulation geometries investigated in this study. It can be seen that the concave wall geometry results in the most effective power conversion, with a high efficiency peak and a broad capture bandwidth. However, the other two geometries, i.e. the convex parabolic wall and the oblique wall exhibit advantageous behaviour in generating multiple localised wave focussed positons which may be favourable for the deployment of a wave energy capture array system.

V. Conclusion

This study has presented the results of a numerical model investigation on the wave focussing effects and power capture by an OWC positioned adjacent to three varying topology reflecting walls. The wave focussing mechanism has been described and the focussing efficacy of the three reflecting walls has been qualitatively described. It is found that the concave parabolic wall is effective in focussing the wave energy to a single point which will benefit the installation of a single WEC device. The oblique wall geometry generates a more uniformly distributed wave focussing arrangement which oscillates with a higher frequency befitting the deployment of a WEC array. The study demonstrates that it is possible to manipulate the hydrodynamic wave field to maximise power capture by installing intelligently designed wave reflecting walls. Whilst this research presents the results of a nascent study on wave focussing, further investigations are required to analyse the wave focussing mechanism and to develop a more robust method to quantitatively characterise the energy focussing capacity of the reflecting walls.

References

[1] Mork, G.; Barstow, S.; Kabuth, A.; Pontes, M.T. Assessing the global wave energy potential. In Proceedings of the ASME 2010 29th International Conference on Ocean, Offshore and Arctic Engineering, Shanghai, China, 6–11 June 2010; pp. 447–454.

[2] Ciappi L, Cheli L, Simonetti I, Bianchini A, Manfrida G, Cappietti L. Wave-to-Wire Model of an Oscillating-Water-Column Wave Energy Converter and Its Application to Mediterranean Energy Hot-Spots. *Energies*. 2020; 13(21):5582. https://doi.org/10.3390/en13215582.

[3] EA-OES (2023), Annual Report: An Overview of Ocean Energy Activities in 2022.

[4] Babarit, A., 2015. A database of capture width ratio of wave energy converters. Renew. Energy 80, 610–628. http://dx.doi.org/10.1016/j.renene.2015.02.049.

[5] Zhang C, Ning D. Hydrodynamic study of a novel breakwater with parabolic openings for wave energy harvest. Ocean Eng 2019;182:540–51.

[6] Ren J, Jin P, Liu Y, Zang J. Wave attenuation and focusing by a parabolic arc pontoon breakwater. Energy 2021;217:119405.

[7] Zhou B, Zheng Z, Jin P, Wang L, Zang J. Wave attenuation and focusing performance of parallel twin parabolic arc floating breakwaters. Energy 2022;260: 125164.

[8] B. Zhou, Z. Zheng, Q. Zhang, P. Jin, L. Wang, D. Ning, Wave attenuation and amplification by an abreast pair of floating parabolic breakwaters, Energy 271 (2023) 127077, https://doi.org/10.1016/j.energy.2023.127077.